

# 2D Hybrid Architectures Constructed from Two Kinds of Polyoxovanadates as Efficient Heterogeneous Catalysts for Cyanosilylation and Knoevenagel Condensation

Haiyan An,\* Jie Zhang, Shenzhen Chang, Yujiao Hou, and Qingshan Zhu

Cite This: <https://dx.doi.org/10.1021/acs.inorgchem.0c00999>

Read Online

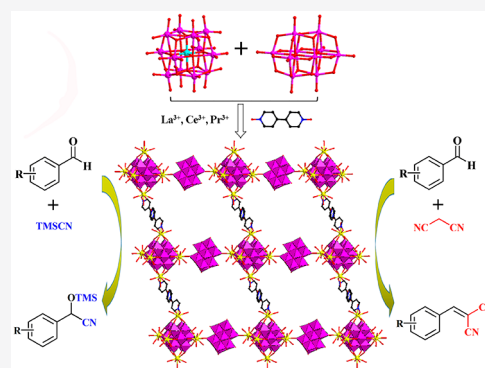
ACCESS |

Metrics & More

Article Recommendations

Supporting Information

**ABSTRACT:** The design of heterogeneous catalysts for highly efficient catalysis for cyanosilylation reactions and Knoevenagel condensations is greatly significant, due to the important application of their products in industry. Herein, five hybrid compounds constructed from two types of polyoxovanadates,  $[\text{MV}_{12}\text{O}_{38}]^{12-}$  ( $\text{M} = \text{Ni}, \text{Mn}$ ) and  $[\text{V}_{10}\text{O}_{28}]^{6-}$ , were successfully synthesized as heterogeneous catalysts for both reactions, which are  $\{(\text{dpdo})[\text{Ln}_2(\text{H}_2\text{O})_9(\text{dpdo})][\text{Ln}(\text{H}_2\text{O})_5][\text{Ln}(\text{H}_2\text{O})_4]_2[\text{V}_{10}\text{O}_{28}][\text{NiV}_{12}\text{O}_{38}]\cdot n\text{H}_2\text{O}\}$  (**1**,  $\text{Ln} = \text{La}$ ,  $n = 23$ ; **2**,  $\text{Ln} = \text{Ce}$ ,  $n = 27$ ; **3**,  $\text{Ln} = \text{Pr}$ ,  $n = 27$ ;  $\text{dpdo} = 4,4'$ -bipyridine  $N,N'$ -dioxide) and  $\{(\text{dpdo})[\text{Ln}_2(\text{H}_2\text{O})_9(\text{dpdo})][\text{Ln}(\text{H}_2\text{O})_5][\text{Ln}(\text{H}_2\text{O})_4]_2[\text{V}_{10}\text{O}_{28}][\text{MnV}_{12}\text{O}_{38}]\cdot 27\text{H}_2\text{O}\}$  (**4**,  $\text{Ln} = \text{La}$ ; **5**,  $\text{Ln} = \text{Pr}$ ). These compounds were characterized by IR spectroscopy, elemental analysis, TG analysis and X-ray diffraction (single crystal and powder) etc. Compounds **1–5** have similar 2D hybrid structures, in which isopolyvanadate  $[\text{V}_{10}\text{O}_{28}]^{6-}$  and heteropolyvanadate  $[\text{MV}_{12}\text{O}_{38}]^{12-}$  are linked together by hydrated  $\text{Ln}^{3+}$  cations and  $\text{Ln}$ - $\text{dpdo}$  coordination complexes. Polyoxovanadates  $[\text{V}_{10}\text{O}_{28}]^{6-}$  and  $[\text{MV}_{12}\text{O}_{38}]^{12-}$  both originate from the transformation of the  $[\text{MV}_{13}\text{O}_{38}]^{7-}$  raw material. This kind of extended structure containing isopolyvanadate and heteropolyvanadate has never been reported hitherto. Because of the Lewis acidity of the  $\text{Ln}^{3+}$  cation and the Lewis basicity of the polyoxovanadates, all five compounds exhibit excellent catalytic performance in cyanosilylation and Knoevenagel condensation reactions. Especially, compound **3**, with a  $\text{Pr}^{3+}$  cation, displayed the best catalytic results. Furthermore, these catalysts exhibit a truly heterogeneous nature and good recyclability.



## INTRODUCTION

The cyanosilylation reaction of aldehydes/ketones with trimethylsilyl cyanide (TMSCN) is one of the important reactions for C–C bond formation, because this reaction produces versatile cyanohydrins which can be used to produce  $\alpha$ -hydroxy acids,  $\alpha$ -hydroxy aldehydes,  $\beta$ -amino alcohols, etc.<sup>1,2</sup> Knoevenagel condensation is another crucial reaction for forming C–C bonds, by adding aldehydes/ketones to active methylene hydrogen compounds, which has been widely used in the syntheses of fine chemicals and pharmaceutical products.<sup>3,4</sup> Thus, the exploration of efficient catalysts for cyanosilylation reactions and Knoevenagel condensations is a very significant topic. So far, some Lewis acid catalysts which can activate the carbonyl substrates as electrophilic catalysts<sup>5–7</sup> and Lewis base catalysts which can nucleophilically activate TMSCN or methylene compounds<sup>8,9</sup> have been developed for both reactions. However, the reported catalysts have obvious drawbacks: (i) homogeneous catalysts with high efficiency are difficult to recover, (ii) heterogeneous catalysts have low efficiency and yield, and (iii) high temperature and toxic solvents are commonly used. Currently, the search for high-efficiency heterogeneous catalysts which can promote cyanosilylation reactions and Knoevenagel condensations

under mild conditions remains challenging but is highly desirable.

Polyoxometalates (POMs) are well-known anionic metal oxides with Mo, V, W, etc. in their highest oxidation states, and they have very attractive applications in catalysis owing to their thermal and oxidative stability in comparison with organo-catalysts and organometallic catalysts.<sup>10–12</sup> A large number of POMs have been used as redox catalysts for efficiently catalyzing the oxidation of sulfides, water, and various olefins or as acid catalysts for the hydrolysis of esters etc.<sup>13–17</sup> In contrast, there have been few examples of POMs catalyzing cyanosilylation reactions and Knoevenagel condensations up to now, which mainly focused on polyoxotungstates and polyoxomolybdates.<sup>18–20</sup> By virtue of the pioneering work of Mizuno, Song, Niu, and other research groups, some lacunary POMs with high negative charges were reported as Lewis base

Received: April 4, 2020

catalysts to promote the cyanosilylation reaction or Knoevenagel condensation.<sup>9,21–23</sup> However, for these lacunary POMs, the conversions of both catalytic reactions still need to be improved. Then, lanthanide (Ln) or transition-metal cations, with good Lewis acid ability, were combined with polyoxoanions to catalyze both reactions. For example, the Ln-substituted lacunary Keggin POMs  $[\{Y(H_2O)_2\}_2(\gamma-SiW_{10}O_{36})_2]^{10-}$  and  $[\{Ln(H_2O)_2(acetone)\}_2(\gamma-SiW_{10}O_{36})_2]^{10-}$  (Ln = Nd<sup>3+</sup>, Eu<sup>3+</sup>, Gd<sup>3+</sup>, Tb<sup>3+</sup>, Dy<sup>3+</sup>, Y<sup>3+</sup>) were first found by Mizuno and co-workers as homogeneous catalysts for efficiently catalyzing the cyanosilylation reaction of aldehydes/ketones.<sup>24,25</sup> A novel hybrid architecture containing lacunary  $[H_2W_{11}O_{38}]^{8-}$  linked by Cu-organic fragments,  $[Cu_2(bpy)(H_2O)_{5.5}]_2[H_2W_{11}O_{38}] \cdot 3H_2O \cdot 0.5SCH_3CN$ , was prepared by Niu's group, showing good performance in heterogeneously catalyzing the cyanosilylation reaction.<sup>22</sup> Our group also reported some hybrid species based on  $[Co_2Mo_{10}H_4O_{38}]^{6-}$ ,  $[PW_{10}Ti_2O_{40}]^{7-}$ , or  $[PW_{11}LnO_{39}]^{4-}$  polyoxoanion with lanthanide cations as linkers, which exhibit good catalytic activity for heterogeneously catalyzing the cyanosilylation reaction under solvent-free conditions.<sup>26–28</sup> Taking account of research status of POM-based catalysts, it is necessary to explore new hybrid materials constructed from highly negatively charged POMs linked by lanthanide groups, which can heterogeneously and high-efficiently catalyze both reactions under mild conditions.

Polyoxovanadates (POVs) seized our attention, not only because vanadium atom has the flexible coordination geometry, but also POVs commonly have good catalytic ability and high negative charges such as isopolyvanadate ( $[V_{10}O_{28}]^{6-}$ ), and heteropolyvanadate with various central heteroatoms ( $[PV_{14}O_{42}]^{9-}$ ,  $[MnV_{13}O_{38}]^{7-}$ ). So far, some success has been achieved in directly introducing lanthanides into one kind of POV, including  $H[Ln(H_2O)_4]_2[MnV_{13}O_{38}] \cdot 9NMP \cdot 17H_2O$  (Ln = La<sup>3+</sup>, Ce<sup>3+</sup>; NMP = N-methyl-2-pyrrolidone),  $H[\{Ln_2(C_6H_5NO_2)_3(H_2O)_6\}][MnV_{13}O_{38}] \cdot C_6H_5NO_2 \cdot 10H_2O$  (Ln = La<sup>3+</sup>, Ce<sup>3+</sup>;  $C_6H_5NO_2$  = isonicotinic acid),  $\{[Ln(H_2O)_6]_2As_8V_{14}O_{42}(SO_3)] \cdot 8H_2O$  (Ln = La<sup>3+</sup>, Ce<sup>3+</sup>, Sm<sup>3+</sup>),  $(TBA)_2[Ln(V_{12}O_{32}(Cl))(H_2O)_2(CH_3CN)_2]$ ,  $(Et_4N)_6[LnV_9O_{27}]$ ,  $\{[V_{12}O_{32}(Cl)](LnPc)\}^{4-}$  (Pc = phthalocyanine), etc.<sup>29–34</sup> Two kinds of POV structural units in one compound will lead to unique structures, which will produce interesting catalytic properties. However, there is an enormous challenge to build compounds containing two kinds of POM structures, owing to the unclear formation mechanism of POMs. Until now, very few compounds containing two kinds of POM structures have been reported, which show excellent catalytic performances in the decontamination of chemical warfare agent simulants or photocatalytic hydrogen and oxygen generation.<sup>17,35</sup> To the best of our knowledge, no compounds containing two kinds of POMs have been used to catalyze the formation of C–C bonds to date, let alone POVs. Consequently, the synthesis of compounds containing two kinds of POVs and lanthanides is especially promising in catalyzing cyanosilylation reactions and Knoevenagel condensations.

Herein, we obtain five new hybrid compounds containing two types of polyoxovanadates,  $[V_{10}O_{28}]^{6-}$  and  $[MnV_{12}O_{38}]^{12-}$  (M = Ni<sup>4+</sup>, Mn<sup>4+</sup>), by carefully adjusting the reaction conditions of the  $[MnV_{13}O_{38}]^{7-}$  mother solution:  $\{(dpdo)-[Ln_2(H_2O)_9(dpdo)][Ln(H_2O)_5]_2[Ln(H_2O)_4]_2[V_{10}O_{28}][NiV_{12}O_{38}] \cdot nH_2O\}$  (**1**, Ln = La, n = 23; **2**, Ln = Ce, n = 27; **3**, Ln = Pr, n = 27; dpdo = 4,4'-bipyridine N,N'-dioxide) and

$\{(dpdo)[Ln_2(H_2O)_9(dpdo)][Ln(H_2O)_5]_2[Ln(H_2O)_4]_2[V_{10}O_{28}][MnV_{12}O_{38}] \cdot 27H_2O\}$  (**4**, Ln = La; **5**, Ln = Pr). In these compounds,  $[V_{10}O_{28}]^{6-}$  and  $[MnV_{12}O_{38}]^{12-}$  polyoxoanions are joined together by lanthanide cations and Ln-dpdo coordination fragments to yield a 2D hybrid network. Interestingly, these compounds display high catalytic activities for catalyzing the cyanosilylation reaction and Knoevenagel condensation under mild conditions; in particular, compound **3** showed the best catalytic performance (99.6% yield for cyanohydrin trimethylsilyl ether within 3 h, 99.7% yield for 2-benzylidenemalononitrile within 0.5 h). Furthermore, these compounds are indeed heterogeneous catalysts and can retain their high catalytic activities and stability of their structures after recycling. To our knowledge, these compounds are the first POVs that have been applied for cyanosilylation and Knoevenagel condensation reactions, as well as the first examples of extended structures containing isopolyvanadate and heteropolyvanadate.

## EXPERIMENTAL SECTION

**Materials.**  $K_7MnV_{13}O_{38} \cdot 18H_2O$ ,  $K_7NiV_{13}O_{38} \cdot 18H_2O$ , and  $K_4Na_2V_{10}O_{28} \cdot 10H_2O$  were prepared following the literature methods<sup>36,37</sup> and characterized by IR. All other reagents were purchased directly from commercial sources and were no longer purified.

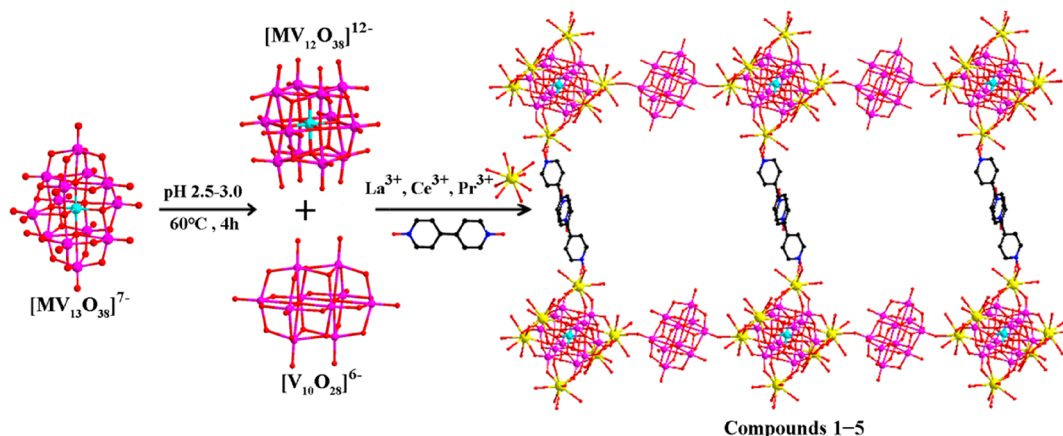
**Physical Measurements.** A PerkinElmer 2400 CHN elemental analyzer was used to analyze the C, H, and N elements. A PLASMA-SPEC (I) ICP atomic emission spectrometer was used to analyze the metal ions of Ni, Mn, V, La, Ce, and Pr. IR spectra were measured on an Alpha Centaur FT-IR spectrophotometer in a range from 400 to 4000 cm<sup>-1</sup> with KBr pellets. PXRD patterns of the samples were measured on a Rigaku Dmax 2000 X-ray instrument with Cu K $\alpha$  radiation ( $\lambda$  = 0.154 nm) with  $2\theta$  varying from 5 to 60° at 298 K. A PerkinElmer TGA instrument was used to measure TG data in flowing N<sub>2</sub> from 30 to 800 °C. A Hitachi U-3900 spectrophotometer was used to obtain UV–vis spectra at room temperature. The GC analyses were performed on a Techcomp GC-7900 instrument with a flame ionization detector (FID) equipped with an SE-54 column (internal diameter 0.32 mm, length 30 m).

**Synthesis.**  $\{(dpdo)[La_2(H_2O)_9(dpdo)][La(H_2O)_5]_2[La(H_2O)_4]_2[V_{10}O_{28}][NiV_{12}O_{38}] \cdot 23H_2O\}$  (**1**).  $K_7NiV_{13}O_{38} \cdot 18H_2O$  (0.0577 g, 0.03 mmol) and  $La(NO_3)_3$  (0.065 g, 0.2 mmol) were added to 10 mL of water in turn. A 1 M HNO<sub>3</sub> solution was used to adjust the pH value of the solution to 2.9. After the solution was heated for 1 h at 60 °C under water bath conditions, a 5 mL aqueous solution of dpdo (0.1 mmol) was added. The solution was continuously heated for 3 h at 60 °C. Then, red block crystals were obtained in 2 weeks after filtration. The crystals were collected, washed with anhydrous ethanol, and dried in air at room temperature before characterization and catalytic testing. Yield: 25.7% (based on  $K_7NiV_{13}O_{38} \cdot 18H_2O$ ). Anal. Calcd for **1**: H, 2.67; C, 5.52; N, 1.29; O, 44.18; Ni, 1.36; V, 25.82; La, 19.18. Found: H, 2.73; C, 5.39; N, 1.41; O, 44.01; Ni, 1.44; V, 25.54; La, 18.95. FTIR data (cm<sup>-1</sup>): 3336 (s), 1470 (m), 1424.6 (w), 1223.7 (m), 1178 (m), 1110 (w), 906 (vs), 621.8 (s), 516.9 (w), 442.7 (m).

$\{(dpdo)[Ce_2(H_2O)_9(dpdo)][Ce(H_2O)_5]_2[Ce(H_2O)_4]_2[V_{10}O_{28}][NiV_{12}O_{38}] \cdot 27H_2O\}$  (**2**). The synthesis method of **2** was similar to that of **1** except that  $Ce(NO_3)_3 \cdot 6H_2O$  (0.0868 g, 0.2 mmol) was used instead of  $La(NO_3)_3$  (0.065 g, 0.2 mmol). Red block crystals of **2** were harvested after 3 weeks of growth. Yield: 19.1% (based on  $K_7NiV_{13}O_{38} \cdot 18H_2O$ ). Anal. Calcd for **2**: H, 2.80; C, 5.42; N, 1.27; O, 43.39; Ni, 1.33; V, 25.35; Ce, 18.98. Found: H, 2.63; C, 5.27; N, 1.46; O, 43.12; Ni, 1.53; V, 25.22; Ce, 18.70. FTIR data (cm<sup>-1</sup>): 3340 (s), 1424.3 (w), 1224 (m), 1180 (m), 1111 (w), 908 (vs), 622.4 (s), 515 (w), 445.4 (m).

$\{(dpdo)[Pr_2(H_2O)_9(dpdo)][Pr(H_2O)_5]_2[Pr(H_2O)_4]_2[V_{10}O_{28}][NiV_{12}O_{38}] \cdot 27H_2O\}$  (**3**). The synthesis method of **3** was similar to that of **1** except that  $PrCl_3$  (0.0494 g, 0.2 mmol) was used instead of  $La(NO_3)_3$  (0.065 g, 0.2 mmol). Red block crystals of **3** were harvested after 2 weeks of

Scheme 1. Schematic Representation of the Formation Processes for Compounds 1–5



growth. Yield: 22.7% (based on  $K_7NiV_{13}O_{38} \cdot 18H_2O$ ). Anal. Calcd for 3: H, 2.80; C, 5.42; N, 1.26; O, 44.78; Ni, 1.33; V, 25.33; Pr, 19.08. Found: H, 2.69; C, 5.61; N, 1.47; O, 44.47; Ni, 1.55; V, 25.05; Pr, 18.88. FTIR data ( $cm^{-1}$ ): 3341.3 (s), 1473 (m), 1424.3 (w), 1224 (m), 1178.8 (m), 1114 (w), 910 (vs), 624 (s), 515.5 (w), 443.1 (m).  $\{(dpdo)[La_2(H_2O)_9(dpdo)][La(H_2O)_5]_2[La(H_2O)_4]_2[V_{10}O_{28}][MnV_{12}O_{38}] \cdot 27H_2O\}$  (4). The synthesis method of 4 was similar to that of 1 except that  $K_7MnV_{13}O_{38} \cdot 18H_2O$  (0.0567 g, 0.03 mmol) was used instead of  $K_7NiV_{13}O_{38} \cdot 18H_2O$  (0.0577 g, 0.03 mmol) and the pH value of the mixture was about 2.7. Red block crystals of 4 were obtained in 3 weeks after filtration. Yield: 18.4% (based on  $K_7MnV_{13}O_{38} \cdot 18H_2O$ ). Anal. Calcd for 4: H, 2.81; C, 5.44; N, 1.27; O, 44.94; Mn, 1.24; V, 25.42; La, 18.88. Found: H, 2.63; C, 5.67; N, 1.45; O, 44.70; Mn, 1.48; V, 25.24; La, 18.66. FTIR data ( $cm^{-1}$ ): 3376.9 (s), 1469.5 (m), 1423.6 (w), 1216.7 (m), 1178.8 (m), 1116.8 (w), 912 (vs), 618 (s), 516.7 (w), 439 (m).

$\{(dpdo)[Pr_2(H_2O)_9(dpdo)][Pr(H_2O)_5]_2[Pr(H_2O)_4]_2[V_{10}O_{28}][MnV_{12}O_{38}] \cdot 27H_2O\}$  (5). The synthesis method of 5 was similar to that of 4 except that  $PrCl_3$  (0.0494 g, 0.2 mmol) was used instead of  $La(NO_3)_3$  (0.065 g, 0.2 mmol) and the pH of the solution was 2.7. Red block crystals of 5 were harvested after 3 weeks of growth. Yield: 19.6% (based on  $K_7MnV_{13}O_{38} \cdot 18H_2O$ ). Anal. Calcd for 5: H, 2.80; C, 5.42; N, 1.27; O, 44.82; Mn, 1.24; V, 25.35; Pr, 19.10. Found: H, 2.44; C, 5.57; N, 1.39; O, 44.62; Mn, 1.41; V, 25.20; Pr, 18.90. FTIR data ( $cm^{-1}$ ): 3400 (s), 1471.5 (m), 1424.6 (w), 1223.7 (m), 1180.1 (m), 1112.2 (w), 912.5 (vs), 621 (s), 516.5 (w), 440.4 (m).

**X-ray Crystallography.** The crystallographic data of compounds 1–5 were determined using a Bruker Smart CCD diffractometer by  $\omega$  and  $\theta$  scan patterns with Mo K $\alpha$  radiation ( $\lambda = 0.71073$ ). The full-matrix least-squares method on  $F^2$  using SHELXL-2014 software was used to solve all structures.<sup>38,39</sup> In compounds 1–5, except for the partial water molecules of crystallization, all non-hydrogen atoms were anisotropically refined. There is half of a disordered dpdo ligand in all five compounds. In the disordered dpdo ligand, all carbon atoms (C6–C15) and nitrogen atoms (N2, N3) are half-occupied. In 1–5, occupancy factors of some water molecules of crystallization were set to be less than 1 owing to disorder. Other restraints including “DFIX” and “ISOR” were used in order to obtain reasonable atomic positions and thermal parameters in the refinements. The crystallographic data and structural determination details for 1–5 are provided in Table S1.

CCDC reference numbers: 1994401–1994405 for 1–5.

**General Procedure for Cyanosilylation Reactions.** A typical method for the cyanosilylation of an aldehyde compound is as follows: the substrate (0.5 mmol) and 1.0 mol % of the catalyst 1–5 (5  $\mu$ mol) were added to trimethylsilyl cyanide (TMSCN) (1.5 mmol) in a 1.5 mL resin vial without solvent and were stirred under 1 atm and 298 K. The conversion of the product was determined by GC analysis. After the reaction was complete, the catalyst was removed by filtration and the reaction mixture was centrifuged. All products (cyanohydrin trimethylsilyl ether) were confirmed by comparison of

GC retention times and GC/MS spectra with real data. Naphthalene was the internal standard in the reaction process.

**General Procedure for Knoevenagel Condensation.** A typical method for the Knoevenagel condensation of an aldehyde compound is as follows: the substrate (0.5 mmol), 0.6 mol % of the catalyst (3  $\mu$ mol), and DMF (0.2 mL) were placed in a resin vial in turn and the reaction was started after adding malononitrile (1 mmol) to the mixture. The structure of each component in the reaction system was determined by GC/MS, and their contents were determined by the mass concentration given by GC with naphthalene as a reference standard. At the end of the reaction, the catalysts were recovered by filtering, washing, and drying.

## RESULTS AND DISCUSSION

**Synthesis.** The reactivity of  $K_7MV_{13}O_{38} \cdot 18H_2O$  ( $M = Ni^{4+}$ ,  $Mn^{4+}$ ) and lanthanide cations in the presence of the dpdo ligand has been investigated. The five isomorphous hybrid frameworks 1–5 comprised of  $[V_{10}O_{28}]^{6-}$  and  $[MV_{12}O_{38}]^{12-}$  polyoxoanions linked by hydrated  $Ln^{3+}$  cations and  $Ln$ -dpdo coordination complexes are formed (see Scheme 1). They represent the very rare examples of two kinds of polyoxoanions in one structure. In these compounds, isopolyvanadate  $[V_{10}O_{28}]^{6-}$  and heteropolyvanadate  $[MV_{12}O_{38}]^{12-}$  come from the transformation of the raw material  $K_7MV_{13}O_{38} \cdot 18H_2O$  ( $M = Ni^{4+}$ ,  $Mn^{4+}$ ). Numerous parallel experiments demonstrate that the reaction temperature, pH value, heating time, metal cations, and organic ligand are key synthetic parameters for the isolation of compounds 1–5. First, the optimal synthetic temperature for compounds 1–5 is 60  $^{\circ}C$ , meaning that the coexistence of  $[MnV_{12}O_{38}]^{12-}$  and  $[V_{10}O_{28}]^{6-}$  only occurs at about 60  $^{\circ}C$ . If the temperature is 80 or 40  $^{\circ}C$ , no crystals were obtained. The group of Lu and Wang group has reported some compounds containing  $[MnV_{13}O_{38}]^{7-}$  and  $Ln^{3+}/Ln$ -organic coordination complexes, which can be obtained at a temperature lower than 45  $^{\circ}C$ .<sup>40</sup> Liu’s group has synthesized five 2D inorganic structures constructed by the two kinds of polyoxovanadates  $[MV_{12}O_{38}]^{12-}$  ( $M = Ni^{4+}$ ,  $Mn^{4+}$ ) and  $[MV_{13}O_{38}]^{7-}$  and hydrated  $Ln^{3+}$  ( $Ln = La, Ce, Pr$ ), which were obtained at 80  $^{\circ}C$ .<sup>41</sup> The above experimental results reveal that the reaction temperature is a very important factor to determine if the  $[MV_{13}O_{38}]^{7-}$  polyoxoanion can be transformed. Second, the quality of the crystals is obviously affected by the pH values of the reaction solution. In the range of pH 2.5–3.0, block crystals with proper size, regular shape, and high yield could be obtained. If the pH value is higher than 3.0, needlelike crystals that could not be tested by single-crystal



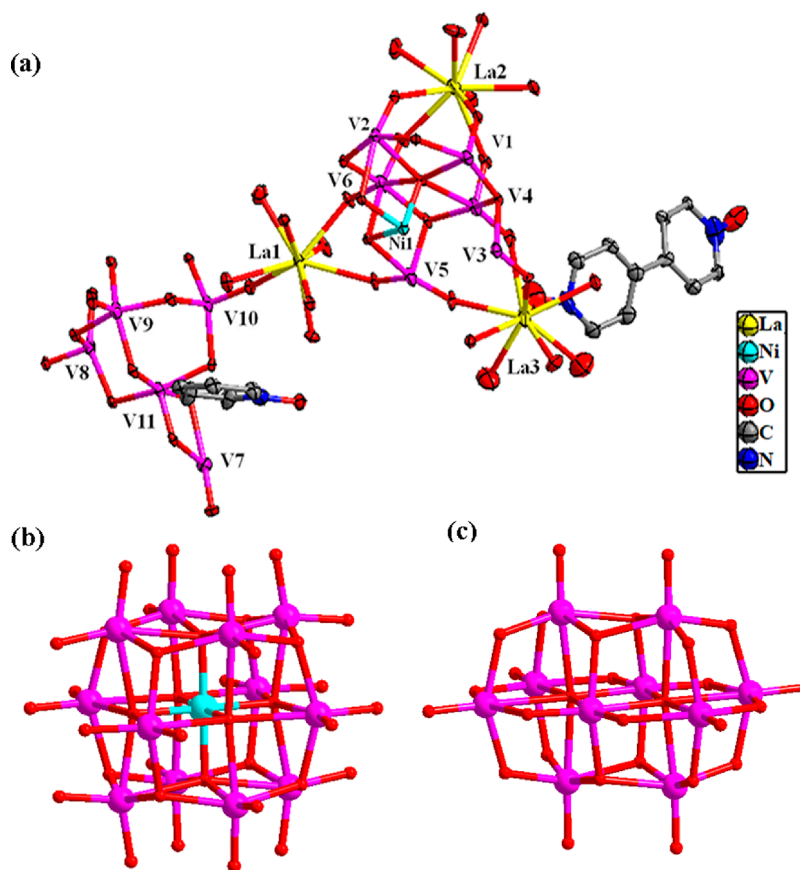


**Figure 1.** (a) ORTEP drawing of compound **1** with thermal ellipsoids at 50% probability. (b) Ball and stick representation of the  $[\text{NiV}_{12}\text{O}_{38}]^{12-}$  polyoxovanadate. (c) Ball and stick representation of the  $[\text{V}_{10}\text{O}_{28}]^{6-}$  polyoxovanadate.

X-ray diffraction will be produced. Third, the effect of heating time on the product structure has been studied. When the heating time is shortened from 4 to 2 h, a new 2D hybrid species (compound **6**) constructed from only the  $[\text{MnV}_{13}\text{O}_{38}]^{7-}$  anion and La-dpdo coordination units was synthesized (see Figure S7). This experimental fact shows that the structural transformation of  $[\text{MV}_{13}\text{O}_{38}]^{7-}$  anion to  $[\text{MnV}_{12}\text{O}_{38}]^{12-}$  and  $[\text{V}_{10}\text{O}_{28}]^{6-}$  needs a longer heating time. Fourth, metal cations can affect the structures of final products. When transition-metal cations such as  $\text{Co}^{2+}$ ,  $\text{Ni}^{2+}$ ,  $\text{Cu}^{2+}$ , and  $\text{Zn}^{2+}$  were used, only amorphous precipitates could be obtained. When other lanthanide cations such as  $\text{Sm}^{3+}$ ,  $\text{Eu}^{3+}$ , and  $\text{Gd}^{3+}$  were added to the system, crystals composed of  $[\text{V}_{10}\text{O}_{28}]^{6-}$  and lanthanide-organic complexes were produced. Finally, the organic ligand dpdo also plays an important role in inducing the successful synthesis of hybrid compounds with two kinds of polyoxovanadates. When other O-donor or N-donor organic ligands such as imidazole, 3-picolinic acid, 4-picolinic acid, and malonic acid were used, no suitable crystals were observed. Therefore, the coordination mode and size of the organic ligand is another key factor in the formation of final products. Obviously, there is still some challenging work that needs to be further exploited, on the transformation mechanism of  $[\text{MV}_{13}\text{O}_{38}]^{7-}$  anion and the related synthetic chemistry.

**Structural Description.** Compounds **1–5** are isomorphous, as shown by single-crystal X-ray diffraction analyses. They have similar unit cell parameters and volumes, crystallizing in the triclinic space group  $P\bar{1}$ . All five compounds display interesting 2D structures constructed from two types of

polyoxovanadates ( $[\text{V}_{10}\text{O}_{28}]^{6-}$ ,  $[\text{MV}_{12}\text{O}_{38}]^{12-}$ ) linked by  $\text{Ln}^{3+}$  cations and Ln-organic coordination complexes. Herein, compound **1** is taken as an example to discuss the structure. The asymmetric unit of **1** is composed of half of a  $[\text{NiV}_{12}\text{O}_{38}]^{12-}$  anion, half of a  $[\text{V}_{10}\text{O}_{28}]^{6-}$  anion, three crystallographically independent  $\text{La}^{3+}$  ions, and two halves of a dpdo ligand (Figure 1a). The structure of  $[\text{NiV}_{12}\text{O}_{38}]^{12-}$  with  $O_h$  symmetry is composed of 13 edge-sharing  $\text{MO}_6$  octahedra ( $M = \text{Ni}, \text{V}$ ), in which  $\text{Ni}^{4+}$  is located on the inversion center. The new type of polyoxovanadate  $[\text{NiV}_{12}\text{O}_{38}]^{12-}$  has rarely been reported to date. Figure 1b shows the structure of the  $[\text{NiV}_{12}\text{O}_{38}]^{12-}$  polyoxovanadate. The Ni–O bond lengths are from 1.861(8) to 1.877(8) Å, and V–O bond lengths are from 1.631(9) to 2.264(8) Å, respectively. The O–Ni–O angles are in the normal octahedral value range, whereas the O–V–O angles range from 71.7(3) to 164.2(4)°, displaying considerable distortion. The  $[\text{V}_{10}\text{O}_{28}]^{6-}$  cluster is comprised of 10 edge-sharing  $\text{VO}_6$  groups, exhibiting a ball-shaped structure (shown in Figure 1c). The V–O bond lengths are from 1.597(9) to 2.325(8) Å, and the O–V–O angles are from 74.3(3) to 175.2(4)°, which are similar to those of other decavanadate clusters reported in the literature.<sup>42,43</sup> The  $[\text{V}_{10}\text{O}_{28}]^{6-}$  polyoxovanadate and  $[\text{NiV}_{12}\text{O}_{38}]^{12-}$  anion are linked together by  $\text{La}^{3+}$  cations.

There are three crystallographically independent  $\text{La}^{3+}$  cations in **1**. All  $\text{La}^{3+}$  cations are nine-coordinated and have a distorted monocapped square-antiprismatic geometry (see Figure S2). The unique La(1) is linked to four water molecules and five terminal oxygen atoms from two polyoxovanadates. La(2) is defined by five water molecules and four terminal

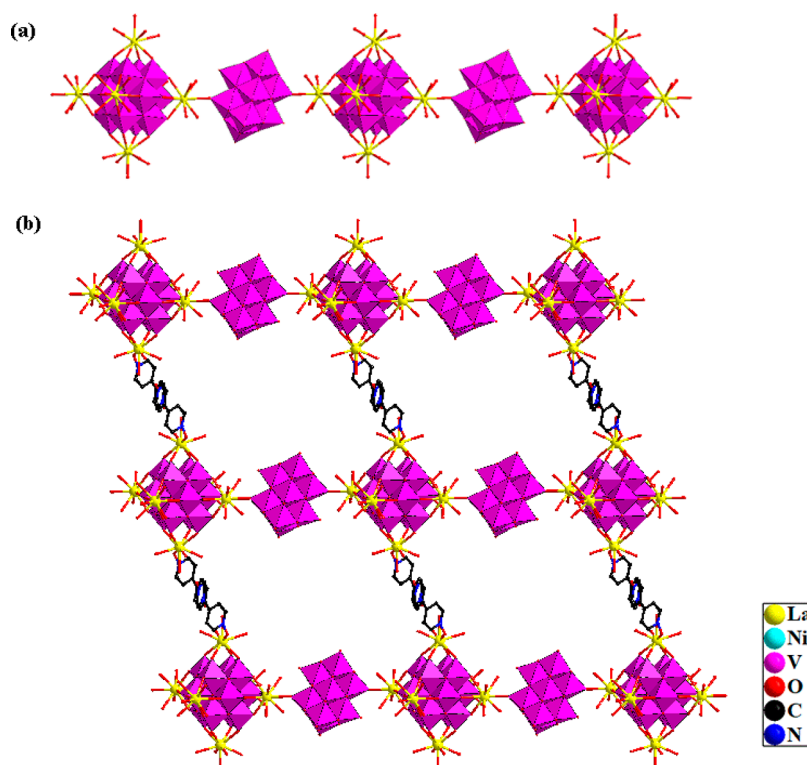


**Figure 2.** (a) Polyhedral and ball and stick view of the 1D chain in **1**. (b) Polyhedral and ball and stick view of the 2D layer in **1**. Color code: La, yellow; V, purple; Ni, light blue; C, gray; N, dark blue; O, red.

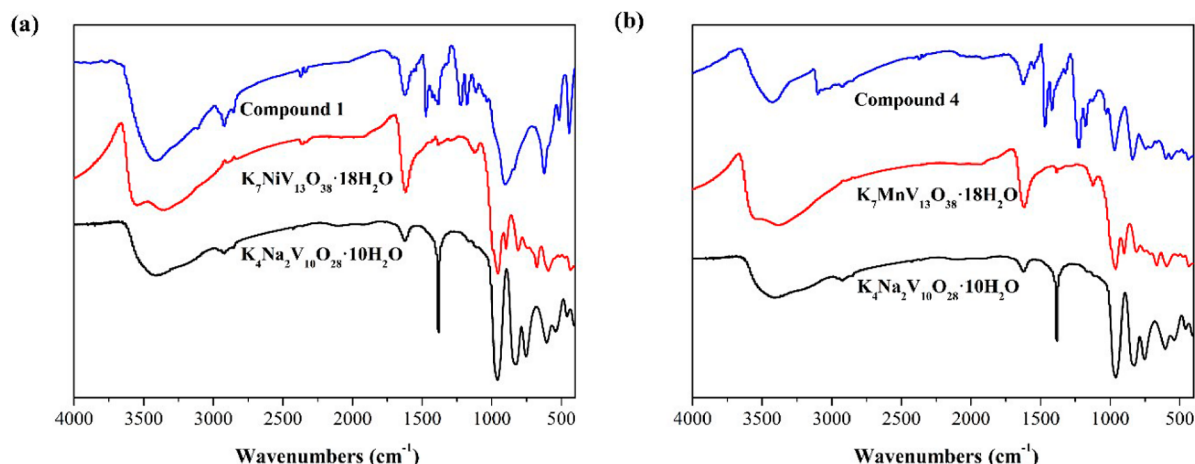


**Figure 3.** (a) IR spectra for **1** (top),  $K_7NiV_{13}O_{38} \cdot 18H_2O$  (middle), and  $K_4Na_2V_{10}O_{28} \cdot 10H_2O$  (bottom). (b) IR spectra for **4** (top),  $K_7MnV_{13}O_{38} \cdot 18H_2O$  (middle), and  $K_4Na_2V_{10}O_{28} \cdot 10H_2O$  (bottom).

oxygen atoms from one polyoxoanion. La(3) is linked to four water molecules, four terminal oxygen atoms from one polyoxoanion, and one oxygen atom from one dpdo molecule. The La–O bond lengths range from 2.508(8) to 2.642(8) Å. There are two half dpdo molecules. The half disordered dpdo ligand acts as a bidentate ligand linking two adjacent La<sup>3+</sup> cations together, and the other dpdo half is an isolated ligand.

In **1**,  $[NiV_{12}O_{38}]^{12-}$  and  $[V_{10}O_{28}]^{6-}$  polyoxoanions are alternately linked by hydrated La<sup>3+</sup> cations to produce a 1D linear chain (see Figure 2a). Neighboring parallel chains are connected together by disordered dpdo ligands to form a 2D layer with large windows (shown in Figure 2b). In the structure, each  $[NiV_{12}O_{38}]^{12-}$  polyoxoanion is connected with two  $[V_{10}O_{28}]^{6-}$  anions by two hydrated La<sup>3+</sup> cations and with

two  $[NiV_{12}O_{38}]^{12-}$  anions by two  $[La_2(H_2O)_9(dpdo)]^{6+}$  units and capped by two additional hydrated La<sup>3+</sup> cations. Herein, the new polyoxoanion  $[NiV_{12}O_{38}]^{12-}$  is reported for the second time, which cannot be separated as an isolated cluster and need to be stabilized by six lanthanide cations surrounding it (Figure S3), similar to the case in the literature.<sup>41</sup> From the view of topology, each  $[NiV_{12}O_{38}]^{12-}$  as a 4-connected node links to two La<sup>3+</sup> cations in the chain and two  $[La_2(H_2O)_9(dpdo)]^{6+}$  clusters to form the 2D structure. Thus, this 2D sheet is a common 4-connected 4<sup>4</sup> net with  $[NiV_{12}O_{38}]^{12-}$  ions as nodes and La<sup>3+</sup> cations and  $[V_{10}O_{28}]^{6-}$  units as linkers (see Figure S4). In the 2D structure, the size of each window is about 17.7 Å × 24.5 Å, which is

Table 1. Cyanosilylation of Various Aldehydes Catalyzed by Compounds 1–5<sup>a</sup>

Catalyst	Substrate	Time (h)	Yield (%) <sup>b</sup>	TON <sup>c</sup>
1		3	98.9	98.9
2		3	93.0	93.0
3		3	99.6	99.6
4		3	89.4	89.4
5		3	94.3	94.3
3		3	99.5	99.5
3		3	99.5	99.5
3		3	99.4	99.4
3		3	99.3	99.3
3		3	99.4	99.4
Blank		3	33.8	33.8
K <sub>7</sub> [NiV <sub>13</sub> O <sub>38</sub> ]·18H <sub>2</sub> O		3	44.2	44.2
K <sub>7</sub> [MnV <sub>13</sub> O <sub>38</sub> ]·18H <sub>2</sub> O		3	35.5	35.5
K <sub>4</sub> Na <sub>2</sub> V <sub>10</sub> O <sub>28</sub> ·10H <sub>2</sub> O		3	70.3	70.3
LaCl <sub>3</sub> ·6H <sub>2</sub> O		3	98.5	98.5
Ce(NO <sub>3</sub> ) <sub>3</sub> ·6H <sub>2</sub> O		3	92.7	92.7
PrCl <sub>3</sub>		3	98.9	98.9

<sup>a</sup>Reaction conditions: 0.5 mmol of aldehydes, 1.5 mmol of TMSCN, 1.0 mol % of catalyst, without solvent, at room temperature for 3 h. <sup>b</sup>Yields were determined by GC using naphthalene as an internal standard. <sup>c</sup>Moles of trimethylsilyl product per mole of catalyst.

large enough to accommodate other polyoxoanions to form a 2-fold interpenetrated 2D network (see Figure S5).

The bond valence sum calculations (BVS)<sup>44</sup> based on the bond lengths observed in compounds 1–5 shows that the

oxidation states of Ni/Mn, V, Ln atoms are +4, +5, and +3, respectively.

**FT-IR Spectroscopy.** The FT-IR spectra of 1–5 are displayed in Figure S8a–e. Their FT-IR spectra are very

similar, which proves that these compounds are isomorphous. Four characteristic peaks at positions of 906, 621.8, 516.9, and 442.7  $\text{cm}^{-1}$  for **1**, 908, 622.4, 515, and 445.4  $\text{cm}^{-1}$  for **2**, 910, 624, 516.5, and 443.1  $\text{cm}^{-1}$  for **3**, 912, 618, 516.7, and 439  $\text{cm}^{-1}$  for **4**, and 912.5, 621, 516.5, and 440.4  $\text{cm}^{-1}$  for **5** are attributed to the stretching vibrations of  $\nu_{\text{as}}(\text{V}=\text{O})$ ,  $\nu_{\text{as}}(\text{V}-\text{O}-\text{V})$ , and  $\nu_{\text{as}}(\text{V}-\text{O}-\text{Ni}/\text{Mn})$ . These characteristic peaks of polyoxovanadates are much different from those of the raw material  $[\text{MV}_{13}\text{O}_{38}]^{7-}$  ( $\text{M} = \text{Ni}, \text{Mn}$ ), indicating that they have different structures.

In comparison with the IR data of  $[\text{MV}_{13}\text{O}_{38}]^{7-}$  or  $[\text{V}_{10}\text{O}_{28}]^{6-}$  (Figure 3), the  $\nu_{\text{as}}(\text{V}=\text{O})$  vibrational bands have different levels of red shifts, perhaps because the strong interactions between  $\text{Ln}^{3+}$  cations and terminal oxygen atoms of polyoxovanadates reduce the  $\text{V}=\text{O}$  bond force constant and lead to a decrease in the  $\text{V}=\text{O}$  vibration frequency. Furthermore, owing to the vibrational coupling of  $[\text{NiV}_{12}\text{O}_{38}]^{12-}$  and  $[\text{V}_{10}\text{O}_{28}]^{6-}$  polyoxoanions, the numbers of characteristic peaks are reduced and the peaks become wide. The peaks at 1470, 1424.6, 1223.7, 1178, and 1110  $\text{cm}^{-1}$  for **1**, 1424.3, 1224, 1180, and 1111  $\text{cm}^{-1}$  for **2**, 1473, 1424.3, 1224, 1178.8, and 1114  $\text{cm}^{-1}$  for **3**, 1469.5, 1423.6, 1216.7, 1178.8, and 1116.8  $\text{cm}^{-1}$  for **4**, and 1471.5, 1424.6, 1223.7, 1180.1, and 1112.2  $\text{cm}^{-1}$  for **5** come from the symmetric and asymmetric stretching vibrations of the dpdo ligand.

**TG Analysis.** Five thermogravimetric curves of **1–5** are given in Figure S9a–e, showing a multistep continuous weight loss process. For compound **1**, the first weight loss of 19.9% from 30 to 200  $^{\circ}\text{C}$  corresponds to the removal of the lattice water molecules and coordinated water molecules (theoretical value: 20.7%). A plateau appears ranging from 200 to 270  $^{\circ}\text{C}$ . Then, the next weight loss after 270  $^{\circ}\text{C}$  is assigned to removal of the ligand molecules and decomposition of the framework. The TG curves of compounds **2–5** display weight loss processes similar to those of compound **1** (shown in Figure S9b–e). For **2–5**, the first weight losses of 20.9%, 20.6%, 21.1%, and 21.0% at 30–200  $^{\circ}\text{C}$ , respectively, agree with the calculated values (21.9%, 21.9%, 22.0%, 22.0%, respectively), due to the removal of lattice and coordinated water molecules. Subsequently, the ligand molecule starts to be lost, and the framework decomposes when the temperature is further increased. Similar weight loss processes can be observed in the reported POV-based hybrid compounds.<sup>45,46</sup>

**PXRD Characterization.** Five PXRD patterns of **1–5** are displayed in Figure S10a–e. The simulated values of these compounds are in agreement with the experimental results, which proves that compounds **1–5** are pure phases. The PXRD patterns of **1–5** are similar, indicating that they are isostructural compounds, which is consistent with the results of crystal structural data.

**UV–Vis Diffuse Reflective Spectroscopy.** The UV–vis diffuse reflectance spectra of compounds **1–5** were measured and displayed in Figure S11. To calculate the absorption ( $A$ ) data, the function  $A = \log(1/R\%)$  is utilized. In the function,  $R$  represents the reflectivity at a given wavelength ( $\lambda$ ). In the UV region from 200 to 400 nm, there are two broad absorption bands centered at 235 and 303 nm in **1**, 229 and 296 nm in **2**, 228 and 302 nm in **3**, 226 and 301 nm in **4**, and 231 and 295 nm in **5**, which can be attributed to the  $\text{O} \rightarrow \text{V}$  charge transfer for polyoxoanions. For compounds **3** and **5**, the curves display an absorption band at 594 nm in the visible region from 400 to 800 nm, which can be assigned to the  $^3\text{H}_4 \rightarrow ^1\text{D}_2$  transitions of  $\text{Pr}^{3+}$  ions.<sup>47</sup>

**Cyanosilylation Study.** The catalytic performances of compounds **1–5** as heterogeneous catalysts were studied in the cyanosilylation reactions of aldehydes with TMSCN under solvent-free conditions. First, benzaldehyde was chosen as the model substrate of cyanosilylation to estimate the catalytic capabilities of all five compounds. The catalytic reaction was run with benzaldehyde (0.5 mmol), TMSCN (1.5 mmol), catalyst (5  $\mu\text{mol}$ ), and naphthalene (internal standard) at room temperature (see Table 1). The results indicate that these five compounds can effectively catalyze the cyanosilylation to give the corresponding cyanohydrin trimethylsilyl ether with 89.4–99.6% yields within 3 h. Compound **3** with a  $\text{Pr}^{3+}$  cation has a higher catalytic activity in comparison to the other isostructural compounds. Thus, compound **3** was selected for a further investigation of the cyanosilylation reaction of various aldehyde compounds. When the substrate is 4-methylbenzaldehyde, 4-fluorobenzaldehyde, or 2-hydroxybenzaldehyde, the yields of products are all over 99%, indicating that the substituent group on the aromatic ring has no prominent effect on the reaction. In general, for a substrate with a large substituent, such as 1-naphthaldehyde, the steric hindrance effect often leads to an unsatisfactory catalytic effect. However, compound **3** exhibited an unusual catalytic ability for the cyanosilylation reaction of 1-naphthaldehyde, and the yield can reach 99.4% after 3 h. These results strongly demonstrate that compound **3** is a highly efficient catalyst for the cyanosilylation reaction of various substrates. This is the first time that polyoxovanadates have exhibited remarkable performance as catalysts in the cyanosilylation reaction.

Some control experiments for the cyanosilylation of benzaldehyde were performed. Without a catalyst, it is difficult to initiate the reaction to produce the target product (Table 1). When the raw material  $\text{K}_4\text{Na}_2\text{V}_{10}\text{O}_{28} \cdot 10\text{H}_2\text{O}$ ,  $\text{K}_7[\text{NiV}_{13}\text{O}_{38}] \cdot 18\text{H}_2\text{O}$ , or  $\text{K}_7[\text{MnV}_{13}\text{O}_{38}] \cdot 18\text{H}_2\text{O}$  is used as a catalyst, the yields are respectively 70.3%, 44.2%, and 35.5% at 3 h, which are far below those of the five compounds. When  $\text{LaCl}_3 \cdot 6\text{H}_2\text{O}$ ,  $\text{Ce}(\text{NO}_3)_3 \cdot 6\text{H}_2\text{O}$ , or  $\text{PrCl}_3$  is used to catalyze the cyanosilylation of benzaldehyde under homogeneous conditions, the yields are 98.5%, 92.7%, and 98.9%, respectively. Because of the synergistic effect of the Lewis base (polyoxoanion) and the Lewis acid ( $\text{Ln}^{3+}$  cations), compounds **1–5** exhibit better catalytic activity. Furthermore, at an equivalent ratio, compounds **1–3** containing  $[\text{NiV}_{12}\text{O}_{38}]^{12-}$  display catalytic results better than those for compounds **4** and **5** containing  $[\text{MnV}_{12}\text{O}_{38}]^{12-}$ , which proves that the composition of the polyoxoanion has an obvious effect on the catalytic activity. This may be due to the fact that the volume of  $[\text{NiV}_{12}\text{O}_{38}]^{12-}$  (87  $\text{\AA}^3$ ) is slightly smaller than that of  $[\text{MnV}_{12}\text{O}_{38}]^{12-}$  (89  $\text{\AA}^3$ ), so that the former polyoxoanion has relatively higher Lewis basicity to promote the catalytic reaction. In addition, experiments on the effect of catalyst content on the reaction results were also conducted (Figure 4). When the catalyst content is less than 1.0 mol %, the yield is lower. When the catalyst content is more than 1.0 mol %, the yield is not significantly increased, and so 1.0 mol % was selected as the optimal amount.

The comparison of compounds **1–5** with other reported POM-based catalysts for the cyanosilylation reaction of aldehydes is shown in Table 2. When our compounds are compared with the homogeneous catalysts  $\text{TBA}_8\text{H}_2[\text{Nd}_2(\text{SiW}_{10}\text{O}_{36})_2] \cdot 7\text{H}_2\text{O}$  (benzaldehyde, 40 min, yield 97%) and  $\text{TBA}_8\text{H}_2[(\text{SiW}_{10}\text{O}_{36})_2]$  (benzaldehyde, 15 min, yield 94%), our compounds (compound **3**, benzaldehyde,



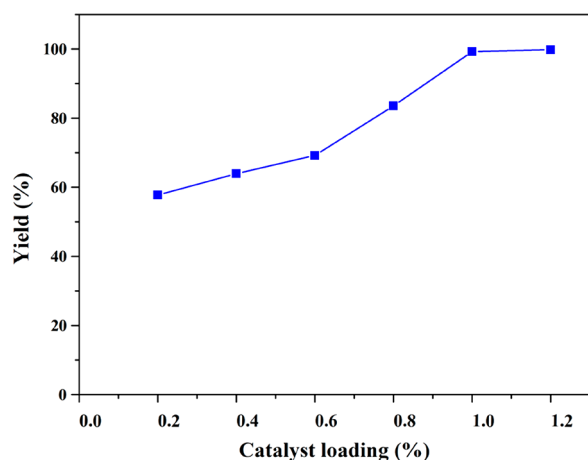


**Figure 4.** Effect of the amount of **3** on the cyanosilylation reaction. Reaction conditions: 0.5 mmol of aldehydes, 1.5 mmol of TMSCN, 5  $\mu$ mol of catalyst (1.0 mol %), without solvent, 3 h, room temperature.

3 h, yield 99.6%) display weaker catalytic activities. However, the homogeneous catalysts have a great disadvantage in that they are difficult to recycle. In comparison with heterogeneous polyoxotungstate catalysts such as  $\text{Cu}_2(\text{bpy})(\text{H}_2\text{O})_{5.5}[\text{H}_2\text{W}_{11}\text{O}_{38}] \cdot 3\text{H}_2\text{O} \cdot 0.5\text{CH}_3\text{CN}$  (benzaldehyde, 24 h, yield 98.1%) and  $\{[\text{Cu}_{12}(\text{pbtz})_2(\text{Hpbtz})_2(\text{OH})_4(\text{H}_2\text{O})_{16}][\text{Na}(\text{H}_2\text{O})\text{P}_5\text{W}_{30}\text{O}_{110}]\} \cdot 16\text{H}_2\text{O}$  (benzaldehyde, 24 h, yield 61.7%),<sup>48</sup> our compounds have better catalytic results as well as a solvent-free advantage. In comparison with heterogeneous polyoxomolybdate catalysts such as  $(\text{NH}_4)_3[\text{Sm}(\text{H}_2\text{O})_6][\text{Co}_2\text{Mo}_{10}\text{H}_4\text{O}_{38}] \cdot 6\text{H}_2\text{O}$  (benzaldehyde, 5 h, yield 98.4%),  $(\text{C}_2\text{N}_2\text{H}_{12})[\text{Sr}(\text{H}_2\text{O})_5][\text{Co}_2\text{Mo}_{10}\text{H}_4\text{O}_{38}] \cdot 2\text{H}_2\text{O}$  (benzaldehyde, 6 h, yield 99%)<sup>49</sup> and  $[\text{Nd}(\text{H}_2\text{O})_5]_2\text{Mo}_6\text{V}_2\text{O}_{26} \cdot 8\text{H}_2\text{O}$  (benzaldehyde, 7 h, yield 96.3%)<sup>50</sup> under solvent-free conditions, our five compounds show stronger catalytic abilities in a shorter reaction time. The TON value of compound **3** is 99.6, which is higher than those of most heterogeneous catalysts based on POMs. It is speculated that the better catalytic activities of **1–5** come from the inclusion of two highly charged POV anions ( $[\text{V}_{10}\text{O}_{28}]^{6-}$ ,  $[\text{MV}_{12}\text{O}_{38}]^{12-}$ ) and lanthanide cations, and their unique 2D structures. Furthermore, the catalytic performance of compound **6**,  $\text{H}[(\text{dpdo})\text{La}(\text{H}_2\text{O})_3]_2[\text{MnV}_{13}\text{O}_{38}] \cdot 14\text{H}_2\text{O}$ , with a  $[\text{MnV}_{13}\text{O}_{38}]^{7-}$  polyoxoanion has been studied. The catalytic result is given in Table 2. Compound **6** can catalyze the

cyanosilylation to give the corresponding cyanohydrin trimethylsilyl ether with 72.4% yield within 3 h, which is far lower than those of compounds **3** and **4**.

In order to study the recyclability and stability of catalysts, compound **3** after the catalytic reaction was filtered, washed, dried, and tested for circulation using benzaldehyde as a model reaction. No obvious reduction in the yield of the product after five cycles (from 99.6% to 95.2%, seen Figure 5a) indicates the excellent cycling stability of the catalyst. The structural stability of the catalyst was tested by performing FT-IR and PXRD on the catalyst before and after the catalytic reaction. PXRD patterns demonstrate that the recovered catalyst is identical in structure with the unused catalyst (Figure S12). FT-IR spectra show that the recovered catalyst has the same characteristic peaks as the unused catalyst (Figure S13), confirming that the catalyst did not undergo structural changes during the catalytic reaction. Furthermore, catalyst **3** was filtered after 30 min of the catalytic reaction, and the filtrate was continued to be stirred (Figure 5b). The product yield increased slightly from 50.4% to 52.9% after 3 h. These results demonstrate that these compounds are genuine heterogeneous catalysts and are capable of maintaining structural integrity. Furthermore, cycle tests in the kinetic regime were performed to confirm the cycling stability of the catalyst at less than 20% conversion. No obvious reduction in the conversion of benzaldehyde in the five cycles indicates the excellent cycling stability of the catalyst (see Figure S18).

Additionally, the IR spectrum of compound **3** after impregnation in the substrate benzaldehyde is displayed in Figure 6a, showing the stretch at  $1689.8\text{ cm}^{-1}$  of  $\text{C}=\text{O}$ , which may come from the red shift from  $1701.4\text{ cm}^{-1}$  of benzaldehyde, and further illustrating that there exists an activation between the substrate and catalyst **3**. Then, a possible mechanism for the cyanosilylation reaction was proposed and is shown in Figure 6b. First, the carbonyl group of aldehyde interacts with the active  $\text{Ln}^{3+}$  sites, thereby improving the electrophilic property of the carboxylic C atom. At the same time, the Si atom of TMSCN interacts with the highly charged POVs, increasing the nucleophilic property of the  $\text{CN}^-$  group. As a consequence, the nucleophilic attack from the  $\text{CN}^-$  group to the carboxylic C atom occurs. A C–C bond is formed. Next, the Si atom of TMSCN further attacks the O atom of the carbonyl group to produce the cyanosilylation product. Meanwhile, the catalyst is recovered.

**Table 2.** Summary of the Catalytic Activity toward Cyanosilylation of Benzaldehyde over Various POMs

catalyst	temp ( $^{\circ}\text{C}$ )	yield (%)	TON <sup>a</sup>	time (h)	ref
<b>3</b>	25	99.6	99.6	3	this work
<b>4</b>	25	89.4	89.4	3	this work
$\text{H}[(\text{dpdo})\text{La}(\text{H}_2\text{O})_3]_2[\text{MnV}_{13}\text{O}_{38}] \cdot 14\text{H}_2\text{O}$	25	72.4	72.4	3	this work
$\text{TBA}_8\text{H}_2[(\text{SiYW}_{10}\text{O}_{36})_2] \cdot 7\text{H}_2\text{O}$	25	94.0	9400	0.25	24
$\text{TBA}_8\text{H}_2[\{\text{Nd}(\text{H}_2\text{O})_2\}_2(\text{SiW}_{10}\text{O}_{36})_2] \cdot 3\text{H}_2\text{O}$	25	99.0	990	0.03	25
$\{[\text{Cu}_2(\text{bpy})(\text{H}_2\text{O})_{5.5}][\text{H}_2\text{W}_{11}\text{O}_{38}] \cdot 3\text{H}_2\text{O} \cdot 0.5\text{CH}_3\text{CN}\}$	rt	98.1	49.05	24	22
$\{[\text{Cu}_{12}(\text{pbtz})_2(\text{Hpbtz})_2(\text{OH})_4(\text{H}_2\text{O})_{16}][\text{Na}(\text{H}_2\text{O})\text{P}_5\text{W}_{30}\text{O}_{110}]\}$	rt	61.7	61.7	24	48
$\text{K}[(\text{H}_2\text{O})_4(\text{Hpbc})_2\text{Ce}][(\text{H}_2\text{O})_5(\text{pic})_2\text{Ce}][\text{PW}_{10}\text{Ti}_2\text{O}_{40}] \cdot 11\text{H}_2\text{O}$	50	99.2	49.6	4	28
$(\text{NH}_4)_3[\text{Sm}(\text{H}_2\text{O})_6][\text{Co}_2\text{Mo}_{10}\text{H}_4\text{O}_{38}] \cdot 6\text{H}_2\text{O}$	25	98.4	49.2	5	26
$(\text{C}_2\text{N}_2\text{H}_{12})[\text{Sr}(\text{H}_2\text{O})_5][\text{Co}_2\text{Mo}_{10}\text{H}_4\text{O}_{38}] \cdot 2\text{H}_2\text{O}$	25	99.0	49.5	6	49
$[\text{Zn}_2(\text{H}_2\text{O})_2(\text{bpe})_3]_2[\text{Co}_2\text{Mo}_{10}\text{H}_4\text{O}_{38}]$	25	99.0	49.5	7	27
$[\text{Nd}(\text{H}_2\text{O})_5]_2\text{Mo}_6\text{V}_2\text{O}_{26} \cdot 8\text{H}_2\text{O}$	25	96.2	96.2	7	50

<sup>a</sup>TON = product (mol)/catalyst (mol).



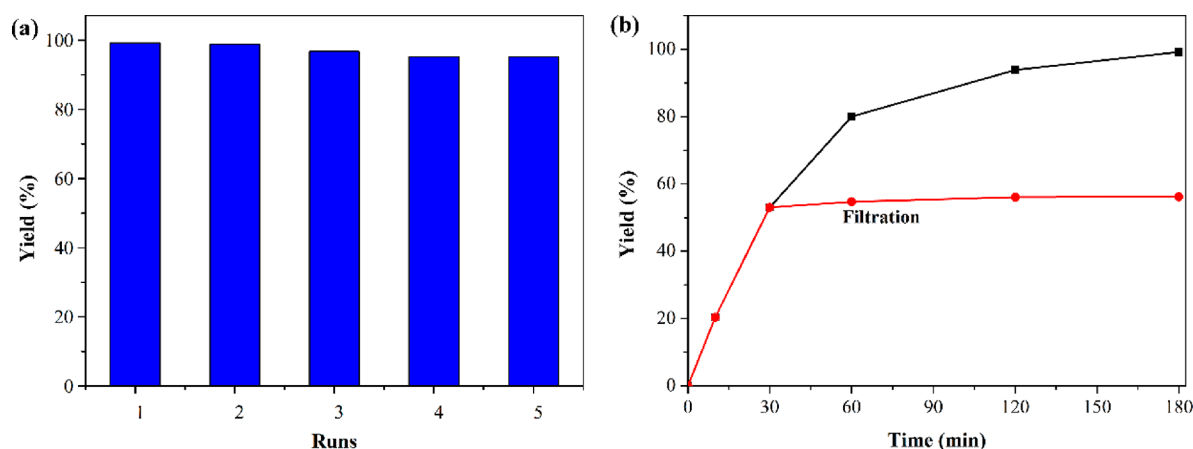


**Figure 5.** (a) Recycling experiments for the cyanosilylation of benzaldehyde over catalyst 3. Reaction conditions: 0.5 mmol of aldehydes, 1.5 mmol of TMSCN, 5  $\mu$ mol of catalyst (1.0 mol %), without solvent, 3 h, room temperature. (b) Yields of product in the cyanosilylation reaction of benzaldehyde catalyzed by 3 (black) and by the filtrate of 3 after 30 min of the reaction (red).

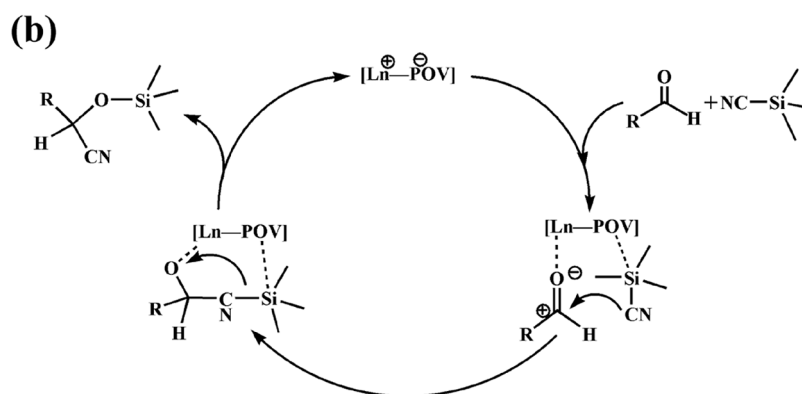
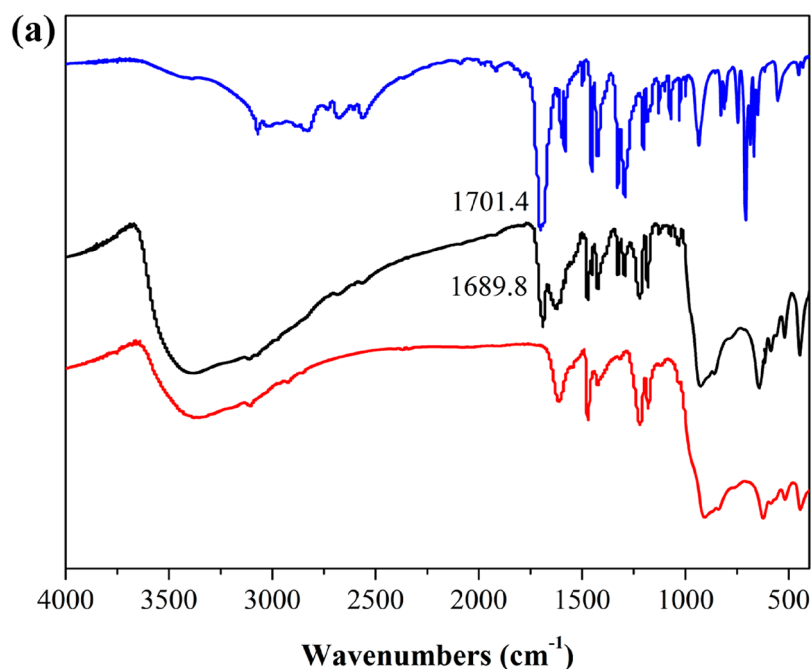
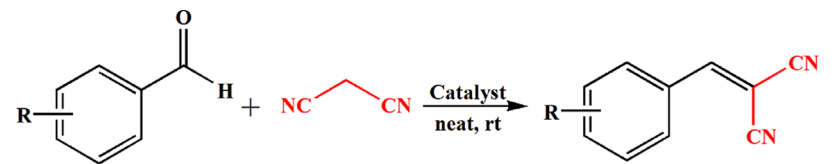


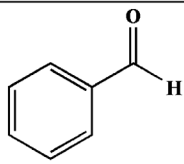
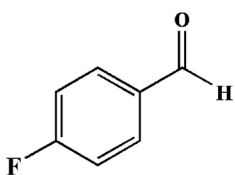
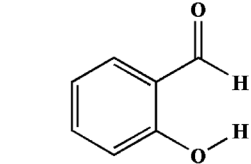
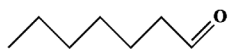
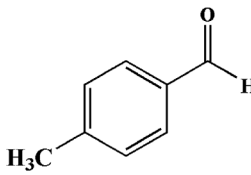
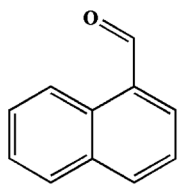
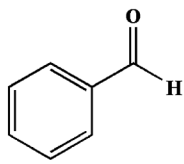
**Figure 6.** (a) IR spectra of 3 (bottom), benzaldehyde (top), and 3 obtained after the absorption of benzaldehyde (middle). (b) The possible catalytic mechanism for the cyanosilylation of aldehydes.

**Knoevenagel Condensation.** Compounds 1–5 were further used as catalysts to study their catalytic performances

for the Knoevenagel reaction. Benzaldehyde was first selected as a model substrate to evaluate the catalytic activities of the

Table 3. Knoevenagel Condensation Catalyzed by Compounds 1–5<sup>a</sup>



Catalyst	Substrate	Time (h)	Yield <sup>b</sup> (%)	TOF <sup>c</sup> (h <sup>-1</sup> )
1		0.5	90.6	301.9
2		0.5	91.8	305.9
3		0.5	99.7	332.3
4		0.5	82.6	275.3
5		0.5	88.2	294.1
3		0.5	99.5	331.5
3		0.5	96.4	321.2
3		0.5	99.3	330.9
3		0.5	98.9	329.5
3		0.5	83.3	277.5
Blank		0.5	40.9	136.4
K <sub>7</sub> [NiV <sub>13</sub> O <sub>38</sub> ]·18H <sub>2</sub> O		0.5	95.4	317.9
K <sub>7</sub> [MnV <sub>13</sub> O <sub>38</sub> ]·18H <sub>2</sub> O		0.5	81.4	271.3
K <sub>4</sub> Na <sub>2</sub> V <sub>10</sub> O <sub>28</sub> ·10H <sub>2</sub> O		0.5	85.5	284.9
LaCl <sub>3</sub> ·6H <sub>2</sub> O		0.5	96.6	322.0
Ce(NO <sub>3</sub> ) <sub>3</sub> ·6H <sub>2</sub> O		0.5	90.2	300.7
PrCl <sub>3</sub>		0.5	98.6	328.7

<sup>a</sup>Reaction conditions: 0.5 mmol of aldehydes, 1 mmol of malononitrile, 0.6 mol % of catalyst (based on substrate), 0.2 mL of solvent, room temperature for 0.5 h. <sup>b</sup>Yields were determined by GC using naphthalene as an internal standard. <sup>c</sup>Moles of condensation product per mole of catalyst per hour.

five compounds. The catalytic reaction was run with benzaldehyde (0.5 mmol), malononitrile (1.0 mmol), catalyst

(3 μmol), DMF (0.2 mL), and a reaction time of 0.5 h at room temperature (see Table 3). It can be seen that the catalytic

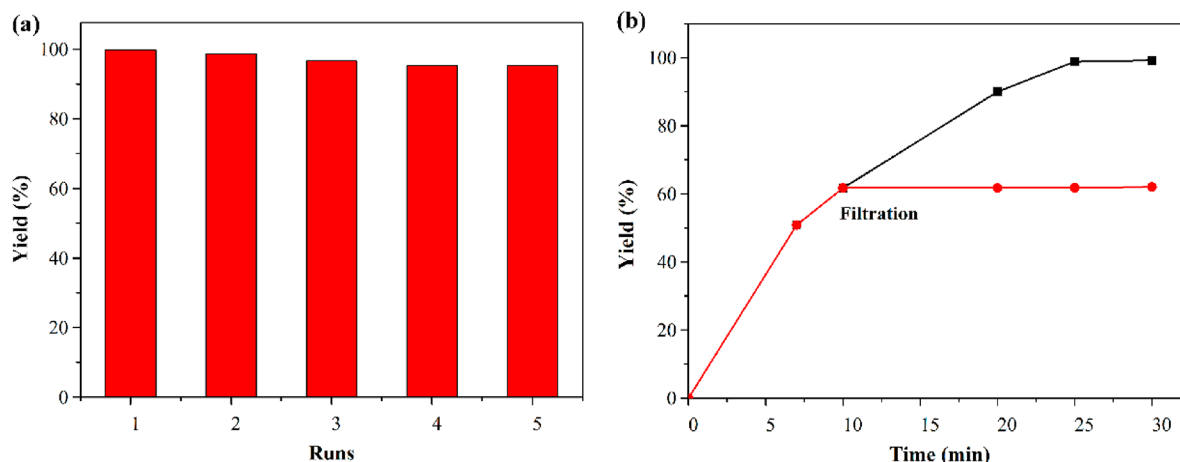


**Figure 7.** (a) Recycling experiments for the Knoevenagel condensation reaction over catalyst **3**. Reaction conditions: 0.5 mmol of aldehydes, 1 mmol of malononitrile, 3  $\mu$ mol of catalyst (0.6 mol %), 0.2 mL of solvent, 0.5 h, room temperature. (b) Yields of product in the Knoevenagel condensation of benzaldehyde catalyzed by **3** (black) and by the filtrate of **3** after 10 min of the reaction (red).

performance of compound **3** is better than those of other isostructural compounds, which is also consistent with the catalytic result drawn from the cyanosilylation reaction. With compound **3** as the catalyst, the yield of 2-benzylidenemalononitrile can reach 99.7%, with a high turnover frequency (TOF) of 332.3  $\text{h}^{-1}$  after 0.5 h, which is faster than those for the previously reported catalysts containing MOFs or POMs (Table S2). In contrast, without a catalyst, benzaldehyde reacted with malononitrile to give a yield of 40.9%, owing to the weak basicity of the DMF solvent. When the raw material  $\text{K}_4\text{Na}_2\text{V}_{10}\text{O}_{28} \cdot 10\text{H}_2\text{O}$ ,  $\text{K}_7[\text{NiV}_{13}\text{O}_{38}] \cdot 18\text{H}_2\text{O}$ , or  $\text{K}_7[\text{MnV}_{13}\text{O}_{38}] \cdot 18\text{H}_2\text{O}$  is used as a homogeneous catalyst, the yields of the corresponding product are respectively 85.5%, 95.4%, and 81.4% within 0.5 h, which indicates that the raw material has lower catalytic activity in comparison to the five compounds **1–5**. When  $\text{LaCl}_3 \cdot 6\text{H}_2\text{O}$ ,  $\text{Ce}(\text{NO}_3)_3 \cdot 6\text{H}_2\text{O}$ , or  $\text{PrCl}_3$  is used to catalyze such a reaction under homogeneous conditions, the yields are 96.6%, 90.2%, and 98.6%, respectively. Thus, the catalysis efficiency for the Knoevenagel condensation reaction can be improved due to the synergy between POV anions and  $\text{Ln}^{3+}$  cations.

With compound **3** as the catalyst, catalytic experiments under different substrate conditions were also carried out. Whether benzaldehyde derivatives with electron-withdrawing groups ( $-\text{F}$ ) or with electron-donating groups ( $-\text{CH}_3$ ) are used, the substrates are fully converted to the catalytic products in excellent yields (98.9–99.5%) with high TOF values (329.5–331.5  $\text{h}^{-1}$ ), revealing that the substituent group on the aromatic ring has no significant effect. When heptanal and 1-naphthaldehyde are used as substrates, the yields of the corresponding products are respectively 99.3% and 83.3%, indicating that compound **3** is an excellent catalyst. The catalytic conditions are optimized by changing the solvents with benzaldehyde used as a model substrate. Table S3 gives the catalytic effect of compound **3** on the reaction in different solvents. When DMF and DMSO are used as solvents, the conversion of benzaldehyde is over 99.5% in 0.5 h. However, through an analysis of GC data and GC-MS data, the selectivity of the product is only 44.84% in DMSO solvent, which is far lower than that in DMF solvent (selectivity, 100%). Consequently, DMF is used as the solvent.

The stability and recyclability of catalysts were also investigated by using benzaldehyde as a substrate. The yield

of the product after five cycles has no obvious decrease (from 99.7% to 95.3%, seen in Figure 7a), which reveals the excellent cycling stability of the catalyst. After the catalyst **3** was removed by filtration at 10 min, the reaction was continued. The product yield increases only slightly from 60.9% to 61.6% after 0.5 h, as shown in Figure 7b. This result further proves the real heterogeneity of the catalyst with no ions leached into the liquid phase. In addition, FT-IR spectra and PXRD patterns of the catalyst **3** before and after the catalytic reactions match well, confirming that the structure of the catalyst did not change (Figures S15 and S16). Furthermore, cycle tests in the kinetic regime were performed to confirm the cycling stability of the catalyst at less than 20% conversion. No obvious reduction in the conversion of benzaldehyde over the five cycles indicates the excellent cycling stability of the catalyst (Figure S18).

## CONCLUSION

In summary, five new hybrid compounds composed of  $[\text{V}_{10}\text{O}_{28}]^{6-}$  and  $[\text{MV}_{12}\text{O}_{38}]^{12-}$  ( $\text{M} = \text{Ni}, \text{Mn}$ ) were successfully synthesized, which represent the first examples where isopolyvanadate and heteropolyvanadate coexist in one extended structure. The five compounds utilizing polyoxovanadate anions as Lewis bases and lanthanide cations as Lewis acids can significantly promote the cyanosilylation reaction and Knoevenagel condensation under mild conditions. Compound **3** containing the  $\text{Pr}^{3+}$  cation displays the best catalytic performance in both C–C formation reactions (yields up to 99.6%). In addition, catalysts **1–5** are genuine heterogeneous catalysts and can keep their high catalytic activities after being recycled five times. The successful synthesis of these hybrid species with two kinds of polyoxovanadates with great catalytic ability should stimulate researchers to enrich the research of POMs in the field of catalyzing C–C bond formation.

## ASSOCIATED CONTENT

### Supporting Information

The Supporting Information is available free of charge at <https://pubs.acs.org/doi/10.1021/acs.inorgchem.0c00999>.

Structural comparison between  $[\text{NiV}_{13}\text{O}_{38}]^{7-}$  and  $[\text{NiV}_{12}\text{O}_{38}]^{12-}$  polyoxoanions, the coordination modes of three  $\text{La}^{3+}$  cations, the coordination environment of

the  $[\text{NiV}_{12}\text{O}_{38}]^{12-}$  polyoxoanion, the 2D topology network, and the 2-fold interpenetrated network in **1**, ORTEP drawings of **2–5**, ORTEP drawing of **6** and the 2D layer in **6**, IR spectra, TG curves, the calculated and experimental PXRD patterns, and UV–vis diffuse reflectance spectra for **1–5**, time profile for the Knoevenagel reaction in the presence of benzaldehyde with and without **3**, PXRD patterns and IR spectra of **3** before and after the cyanosilylation, PXRD patterns and IR spectra of **3** before and after the Knoevenagel reaction, crystal data and structure refinement details for **1–5**, and the effect of different solvents on the Knoevenagel condensation catalyzed by **3** (PDF)

### Accession Codes

CCDC 1994401–1994405 contain the supplementary crystallographic data for this paper. These data can be obtained free of charge via [www.ccdc.cam.ac.uk/data\\_request/cif](http://www.ccdc.cam.ac.uk/data_request/cif), or by emailing [data\\_request@ccdc.cam.ac.uk](mailto:data_request@ccdc.cam.ac.uk), or by contacting The Cambridge Crystallographic Data Centre, 12 Union Road, Cambridge CB2 1EZ, UK; fax: +44 1223 336033.

## AUTHOR INFORMATION

### Corresponding Author

Haiyan An – College of Chemistry, Dalian University of Technology, Dalian 116023, People's Republic of China; [orcid.org/0000-0003-3848-5210](https://orcid.org/0000-0003-3848-5210); Phone: +86-411-84657675; Email: [anh@dlut.edu.cn](mailto:anh@dlut.edu.cn)

### Authors

Jie Zhang – College of Chemistry, Dalian University of Technology, Dalian 116023, People's Republic of China  
Shenzhen Chang – College of Chemistry, Dalian University of Technology, Dalian 116023, People's Republic of China; [orcid.org/0000-0002-8983-9309](https://orcid.org/0000-0002-8983-9309)  
Yujiao Hou – College of Chemistry, Dalian University of Technology, Dalian 116023, People's Republic of China  
Qingshan Zhu – College of Chemistry, Dalian University of Technology, Dalian 116023, People's Republic of China

Complete contact information is available at: <https://pubs.acs.org/10.1021/acs.inorgchem.0c00999>

### Notes

The authors declare no competing financial interest.

## ACKNOWLEDGMENTS

The authors appreciate the financial support from the National Natural Science Foundation of China (21371027, 20901013), the Natural Science Foundation of Liaoning Province (2015020232) and the Fundamental Research Funds for the Central Universities (DUT19LK01, DUT15LN18).

## REFERENCES

- (1) Gregory, R. J. H. Cyanohydrins in nature and the laboratory: biology, preparations, and synthetic applications. *Chem. Rev.* **1999**, *99*, 3649–3682.
- (2) North, M.; Usanov, D. L.; Young, C. Lewis acid catalyzed asymmetric cyanohydrin synthesis. *Chem. Rev.* **2008**, *108*, 5146–5226.
- (3) List, B. Emil Knoevenagel and the roots of aminocatalysis. *Angew. Chem., Int. Ed.* **2010**, *49*, 1730–1734.
- (4) Bigi, F.; Chesini, L.; Maggi, R.; Sartori, G. Montmorillonite KSF as an inorganic, water stable, and reusable catalyst for the

Knoevenagel synthesis of coumarin-3-carboxylic acids. *J. Org. Chem.* **1999**, *64*, 1033–1035.

- (5) Sreekanth, P.; Kim, S. W.; Hyeon, T.; Kim, B. M. A novel mesoporous silica-supported Lewis acid catalyst for C–C Bond formation reactions in water. *Adv. Synth. Catal.* **2003**, *345*, 936–938.
- (6) (a) D'Vries, R. F.; Iglesias, M.; Snejko, N.; Gutierrez-Puebla, E.; Monge, M. A. Lanthanide metal–organic frameworks: searching for efficient solvent-free catalysts. *Inorg. Chem.* **2012**, *51*, 11349–11355. (b) Liu, L.; Han, Z. B.; Wang, S. M.; Yuan, D. Q.; Ng, S. W. Robust molecular bowl-based metal–organic frameworks with open metal sites: size modulation to increase the catalytic activity. *Inorg. Chem.* **2015**, *54*, 3719–3721.
- (7) Jiang, W.; Yang, J.; Liu, Y.; Song, S.; Ma, J. F. A stable porphyrin-based porous metal–organic framework as an efficient solvent-free catalyst for C–C bond formation. *Inorg. Chem.* **2017**, *56*, 3036–3043.
- (8) Denmark, S. E.; Chung, W. Lewis base catalyzed addition of trimethylsilyl cyanide to aldehydes. *J. Org. Chem.* **2006**, *71*, 4002–4005.
- (9) Zhao, S.; Chen, Y.; Song, Y. F. Tri-lacunary polyoxometalates of  $\text{Na}_8\text{H}[\text{PW}_3\text{O}_{34}]$  as heterogeneous Lewis base catalysts for Knoevenagel condensation, cyanosilylation and the synthesis of benzoxazole derivatives. *Appl. Catal., A* **2014**, *475*, 140–146.
- (10) Lv, H.; Geletii, Y. V.; Zhao, C.; Vickers, J. W.; Zhu, G.; Luo, Z.; Song, J.; Lian, T.; Musaev, D. G.; Hill, C. L. Polyoxometalate water oxidation catalysts and the production of green fuel. *Chem. Soc. Rev.* **2012**, *41*, 7572–7589.
- (11) (a) Wang, S. S.; Yang, G. Y. Recent advances in polyoxometalate catalyzed reactions. *Chem. Rev.* **2015**, *115*, 4893–4962. (b) Zhao, J. W.; Li, Y. Z.; Chen, L. J.; Yang, G. Y. Research progress on polyoxometalate-based transition-metal–rare-earth heterometallic derived materials: synthetic strategies, structural overview and functional applications. *Chem. Commun.* **2016**, *52*, 4418–4445.
- (12) (a) Du, D. Y.; Qin, J. S.; Li, S. L.; Su, Z. M.; Lan, Y. Q. Recent advances in porous polyoxometalate-based metal–organic framework materials. *Chem. Soc. Rev.* **2014**, *43*, 4615–4632. (b) Zhang, F. M.; Dong, L. Z.; Qin, J. S.; Guan, W.; Liu, J.; Li, S. L.; Lu, M.; Lan, Y. Q.; Su, Z. M.; Zhou, H. C. Effect of imidazole arrangements on proton-conductivity in metal–organic frameworks. *J. Am. Chem. Soc.* **2017**, *139*, 6183–6189.
- (13) Cronin, L.; Müller, A. From serendipity to design of polyoxometalates at the nanoscale, aesthetic beauty and applications. *Chem. Soc. Rev.* **2012**, *41*, 7333–7334.
- (14) (a) Dolbecq, A.; Dumas, E.; Mayer, C. R.; Mialane, P. Hybrid organic–inorganic polyoxometalate compounds: from structural diversity to applications. *Chem. Rev.* **2010**, *110*, 6009–6048. (b) An, H. Y.; Hou, Y. J.; Wang, L.; Zhang, Y. M.; Yang, W.; Chang, S. Z. Evans–Showell-type polyoxometalates constructing high dimensional inorganic–organic hybrid compounds with copper–organic coordination complexes: synthesis and oxidation catalysis. *Inorg. Chem.* **2017**, *56*, 11619–11632.
- (15) (a) Zhang, J.; Hao, J.; Wei, Y. G.; Xiao, F. P.; Yin, P. C.; Wang, L. S. Nanoscale chiral rod-like molecular triads assembled from achiral polyoxometalates. *J. Am. Chem. Soc.* **2010**, *132*, 14–15. (b) Li, D. D.; Xu, Q. F.; Li, Y. G.; Qiu, Y. T.; Ma, P. T.; Niu, J. Y.; Wang, J. P. A Stable Polyoxometalate-Based Metal–Organic Framework as Highly Efficient Heterogeneous Catalyst for Oxidation of Alcohols. *Inorg. Chem.* **2019**, *58*, 4945–4953.
- (16) (a) Banerjee, A.; Bassil, B. S.; Röscenthaler, G. V.; Kortz, U. Diphosphates and diphosphonates in polyoxometalate chemistry. *Chem. Soc. Rev.* **2012**, *41*, 7590–7604. (b) Hou, Y. J.; An, H. Y.; Zhang, Y. M.; Hu, T.; Yang, W.; Chang, S. Z. Rapid destruction of two types of chemical warfare agent simulants by hybrid polyoxomolybdates modified by carboxylic acid ligands. *ACS Catal.* **2018**, *8*, 6062–6069.
- (17) (a) Dong, J.; Hu, J. F.; Chi, Y. N.; Lin, Z. G.; Zou, B.; Yang, S.; Hill, C. L.; Hu, C. W. A polyoxoniobate–polyoxovanadate double-anion catalyst for simultaneous oxidative and hydrolytic decontamination of chemical warfare agent simulants. *Angew. Chem., Int. Ed.*



- 2017, *S6*, 4473–4477. (b) Han, Q.; Li, Z.; Liang, X. M.; Ding, Y.; Zheng, S. T. Synthesis of a 6-nm-long transition-metal–rare-earth-containing polyoxometalate. *Inorg. Chem.* **2019**, *58*, 12534–12537.
- (18) Li, S. J.; Zhou, Y. F.; Peng, Q. P.; Wang, R. Y.; Feng, X. G.; Liu, S. X.; Ma, X. M.; Ma, N. N.; Zhang, J.; Chang, Y.; Zheng, Z. P.; Chen, X. N. Controllable synthesis and catalytic performance of nanocrystals of rare-earth-polyoxometalates. *Inorg. Chem.* **2018**, *57*, 6624–6631.
- (19) Hayashi, S.; Sasaki, N.; Yamazoe, S.; Tsukuda, T. Superior base catalysis of group 5 hexametalates  $[M_6O_{19}]^{8-}$  ( $M = Ta, Nb$ ) over group 6 hexametalates  $[M_6O_{19}]^{2-}$  ( $M = Mo, W$ ). *J. Phys. Chem. C* **2018**, *122*, 29398–29404.
- (20) Ye, J. J.; Wu, C. D. Immobilization of polyoxometalates in crystalline solids for highly efficient heterogeneous catalysis. *Dalton Trans.* **2016**, *45*, 10101–10112.
- (21) Sugahara, K.; Kimura, T.; Kamata, K.; Yamaguchi, K.; Mizuno, N. A highly negatively charged  $\gamma$ -Keggin germanodecatungstate efficient for Knoevenagel condensation. *Chem. Commun.* **2012**, *48*, 8422–8424.
- (22) Han, Q. X.; Sun, X. P.; Li, J.; Ma, P. T.; Niu, J. Y. Novel isopolyoxotungstate  $[H_2W_{11}O_{38}]^{8-}$  based metal organic framework: as Lewis acid catalyst for cyanosilylation of aromatic aldehydes. *Inorg. Chem.* **2014**, *53*, 6107–6112.
- (23) Hu, T. P.; Zhao, Y. Q.; Jagličić, Z.; Yu, K.; Wang, X. P.; Sun, D. A novel silver(I)-Keggin-polyoxometalate inorganic–organic hybrid: a Lewis acid catalyst for cyanosilylation reaction. *Inorg. Chem.* **2015**, *54*, 7415–7423.
- (24) Kikukawa, Y.; Suzuki, K.; Sugawa, M.; Hirano, T.; Kamata, K.; Yamaguchi, K.; Mizuno, N. Cyanosilylation of carbonyl compounds with trimethylsilyl cyanide catalyzed by an yttrium-pillared silicotungstate dimer. *Angew. Chem., Int. Ed.* **2012**, *51*, 3686–3690.
- (25) Suzuki, K.; Sugawa, M.; Kikukawa, Y.; Kamata, K.; Yamaguchi, K.; Mizuno, N. Strategic design and refinement of Lewis acid–base catalysis by rare-earth-metal-containing polyoxometalates. *Inorg. Chem.* **2012**, *51*, 6953–6961.
- (26) An, H. Y.; Wang, L.; Hu, Y.; Fei, F. Temperature-induced racemic compounds and chiral conglomerates based on polyoxometalates and lanthanides: syntheses, structures and catalytic properties. *CrystEngComm* **2015**, *17*, 1531–1540.
- (27) Fei, F.; An, H. Y.; Xu, T. Q.; Meng, C. G. Syntheses, structures and catalytic properties of organic–inorganic hybrid materials constructed from Evans–Showell-type polyoxometalates and zinc-organic coordination units. *RSC Adv.* **2016**, *6*, 92092–92103.
- (28) An, H. Y.; Zhang, Y. M.; Hou, Y. J.; Hu, T.; Yang, W.; Chang, S. Z.; Zhang, J. J. Hybrid dimers based on metal-substituted Keggin polyoxometalates (metal = Ti, Ln) for cyanosilylation catalysis. *Dalton Trans.* **2018**, *47*, 9079–9089.
- (29) Liu, D.; Lu, Y.; Tan, H. Q.; Chen, W. L.; Zhang, Z. M.; Li, Y. G.; Wang, E. B. Polyoxometalate-based purely inorganic porous frameworks with selective adsorption and oxidative catalysis functionalities. *Chem. Commun.* **2013**, *49*, 3673–3675.
- (30) Liu, D.; Lu, Y.; Tan, H. Q.; Wang, T. T.; Wang, E. B. Series of organic–inorganic hybrid rare earth derivatives based on  $[MnV_{13}O_{38}]^{7-}$  polyoxoanion: syntheses, structures, and magnetic and electrochemical properties. *Cryst. Growth Des.* **2015**, *15*, 103–114.
- (31) Arumuganathan, T.; Das, S. K. Discrete polyoxovanadate cluster into an organic free metal-oxide-based material: syntheses, crystal structures, and magnetic properties of a new series of lanthanide linked-POV compounds  $[\{Ln(H_2O)_6\}_2As_8V_{14}O_{42}(SO_3)] \cdot 8H_2O$  ( $Ln = La^{3+}, Sm^{3+}$ , and  $Ce^{3+}$ ). *Inorg. Chem.* **2009**, *48*, 496–507.
- (32) Cameron, J. M.; Newton, G. N.; Busche, C.; Long, D. L.; Oshio, H.; Cronin, L. Synthesis and characterisation of a lanthanide-capped dodecavanadate cage. *Chem. Commun.* **2013**, *49*, 3395–3397.
- (33) Nishio, M.; Inami, S.; Katayama, M.; Ozutsumi, K.; Hayashi, Y. Lanthanide complexes of macrocyclic polyoxovanadates by  $VO_4$  units: synthesis, characterization, and structure elucidation by X-ray crystallography and EXAFS spectroscopy. *Inorg. Chem.* **2012**, *51*, 784–793.
- (34) Pütt, R.; Qiu, X. K.; Kozłowski, P.; Gildenast, H.; Linnenberg, O.; Zahn, S.; Chiechi, R. C.; Monakhov, K. Y. Self-assembled monolayers of polyoxovanadates with phthalocyaninato lanthanide moieties on gold surfaces. *Chem. Commun.* **2019**, *55*, 13554–13557.
- (35) Shi, D. Y.; Zheng, R.; Liu, C. S.; Chen, D. M.; Zhao, J. W.; Du, M. Dual-functionalized mixed Keggin- and Lindqvist-Type  $Cu_{24}$ -based POM@MOF for visible-light-driven  $H_2$  and  $O_2$  evolution. *Inorg. Chem.* **2019**, *58*, 7229–7235.
- (36) Flynn, C. M.; Pope, M. T. 1:13 Heteropolyvanadates of manganese(IV) and nickel(IV). *J. Am. Chem. Soc.* **1970**, *92*, 85–90.
- (37) Lee, U.; Joo, H. C. Potassium-sodium double salt of decavanadate,  $K_4Na_2[V_{10}O_{28}] \cdot 10H_2O$ . *Acta Crystallogr., Sect. E* **2003**, *E59*, i122–i124.
- (38) Sheldrick, G. M. *SHELXL 97, Program for Crystal Structure Refinement*; University of Göttingen: Göttingen, Germany, 1997.
- (39) Sheldrick, G. M. *SHELXL 97, Program for Crystal Structure Solution*; University of Göttingen: Göttingen, Germany, 1997.
- (40) Liu, D.; Lu, Y.; Li, Y. G.; Tan, H. Q.; Chen, W. L.; Zhang, Z. M.; Wang, E. B. Assembly of trimeric polyoxovanadate aggregates based on  $[MnV_{13}O_{38}]^{7-}$  building blocks and lanthanide cations. *Dalton Trans.* **2013**, *42*, 14445–14453.
- (41) Liu, S. X.; Li, D. H.; Xie, L. H.; Cheng, H. Y.; Zhao, X. Y.; Su, Z. M. Two-dimensional lanthanide heteropolyvanadates of manganese(IV) and nickel(IV) containing two types of heteropoly anions with 1:13 and 1:12 stoichiometry. *Inorg. Chem.* **2006**, *45*, 8036–8040.
- (42) Thomas, J.; Agarwal, M.; Ramanan, A.; Chernovab, N.; Whittingham, M. S. Copper pyrazole directed crystallization of decavanadates: synthesis and characterization of  $\{Cu(pz)_4\}[\{Cu(pz)_3\}_2V_{10}O_{28}]$  and  $(Hpz)_2[\{Cu(pz)_4\}_2V_{10}O_{28}] \cdot 2H_2O$ . *CrystEngComm* **2009**, *11*, 625–631.
- (43) Martin-Caballero, J.; San Jose Wery, A.; Reinoso, S.; Artetxe, B.; San Felices, L.; El Bakkali, B.; Trautwein, G.; Alcaniz-Monge, J.; Vilas, J. L.; Gutierrez-Zorrilla, J. M. A robust open framework formed by decavanadate clusters and copper(II) complexes of macrocyclic polyamines: permanent microporosity and catalytic oxidation of cycloalkanes. *Inorg. Chem.* **2016**, *55*, 4970–4979.
- (44) Brown, I. D.; Altermatt, D. Bond-valence parameters obtained from a systematic analysis of the Inorganic Crystal Structure Database. *Acta Crystallogr., Sect. B: Struct. Sci.* **1985**, *41*, 244–247.
- (45) Zhang, Y. T.; Wang, X. L.; Li, S. B.; Song, B. Q.; Shao, K. Z.; Su, Z. M. Ligand-directed assembly of polyoxovanadate-based metal–organic polyhedra. *Inorg. Chem.* **2016**, *55*, 8770–8775.
- (46) Cao, J. P.; Xue, Y. S.; Li, N. F.; Gong, J. J.; Kang, R. K.; Xu, Y. Lewis acid dominant windmill-shaped  $V_8$  clusters: a bifunctional heterogeneous catalyst for  $CO_2$  cycloaddition and oxidation of sulfides. *J. Am. Chem. Soc.* **2019**, *141*, 19487–19497.
- (47) Huskowska, E.; Porcher, P.; Legendziewicz, J. Electronic spectroscopy ( $Pr^{3+}$ ) and crystal field parameter calculations ( $Eu^{3+}$ ) for complexes of formula  $[Ln(2,2'-bipyridine-1,1'-dioxide)_4](ClO_4)_3$ . *J. Alloys Compd.* **2002**, *341*, 187–192.
- (48) Hu, T. P.; Zhao, Y. Q.; Jagličić, Z.; Yu, K.; Wang, X. P.; Sun, D. Four hybrid materials based on preyssler  $P_5W_{30}$  polyoxometalate and first-row transition-metal complex. *Inorg. Chem.* **2015**, *54*, 7415–7423.
- (49) Hou, Y. J.; An, H. Y.; Ding, B. J.; Li, Y. Q. Evans–Showell-type polyoxometalate constructing novel 3D inorganic architectures with alkaline earth metal linkers: syntheses, structures and catalytic properties. *Dalton Trans.* **2017**, *46*, 8439–8450.
- (50) Fei, F.; An, H. Y.; Meng, C. G.; Wang, L.; Wang, H. L. Lanthanide-supported molybdenum–vanadium oxide clusters: syntheses, structures and catalytic properties. *RSC Adv.* **2015**, *5*, 18796–18805.